



INVERSE-FORWARD METHOD FOR HEAT FLOW ESTIMATION: CASE STUDY FOR THE ARCTIC REGION

Alexey G. Petrunin^{1,2}, Anatoly A. Soloviev^{1,2}, Roman V. Sidorov^{*,1}, and
Alexei D. Gvishiani^{1,2}

¹*Geophysical Center of the Russian Academy of Sciences, 119296 Moscow, Russia*

²*Schmidt Institute of Physics of the Earth of the Russian Academy of Sciences, 123242 Moscow, Russia*

Received 10 July 2022; accepted 9 September 2022; published 12 December 2022.

The heat flow data are important in many aspects including interpretation of various geophysical observations, solutions of important engineering problems, modelling of the ice dynamics, and related environmental assessment. However, the distribution of the direct measurements is quite heterogeneous over the Earth. Different methods have been developed during past decades to create continuous maps of the geothermal heat flow (GHF). Most of them are based on the principle of similarity of GHF values for the lithosphere with comparable age and tectonic history or inversion of magnetic field data. Probabilistic approach was also used to realize this principle. In this paper, we present a new method for extrapolating the GHF data, based on the inversion of a geophysical data set using optimization problem solution. We use the results of inversion of seismic and magnetic field data into temperature and data from direct heat flow measurements. We use the Arctic as the test area because it includes the lithosphere of different ages, types, and tectonic settings. In result, the knowledge of GHF is important here for various environmental problems. The resulting GHF map obtained well fits to the observed data and clearly reflects the lithospheric domains with different tectonic history and age. The new GHF map constructed in this paper reveals some significant features that were not identified earlier. In particular, these are the increased GHF zones in the Bering Strait, the Chukchi Sea and the residual GHF anomaly in the area of the Mid-Labrador Ridge. The latter was active during the Paleogene.

Keywords: geothermal heat flow, Arctic, inversion, optimization, lithosphere

Citation: Petrunin, Alexey G., Anatoly A. Soloviev, Roman V. Sidorov, and Alexei D. Gvishiani (2022), Inverse-forward method for heat flow estimation: case study for the Arctic region, *Russian Journal of Earth Sciences*, Vol. 22, ES6004, doi: 10.2205/2022ES000809.

1 INTRODUCTION

Reliable data on the geothermal heat flow (GHF) are extremely important for many areas of the Earth science. The heat flux well reflects tectonic structure and thermal properties of the crust and lithosphere. In this connection, it is important to construct reliable 3D models of the lithosphere based on a joint interpretation of seismic and gravity data [e.g., [Kaban et al., 2003](#)]. Furthermore, knowledge of the GHF is necessary to table several problems directly related to the human habitat. Indeed, GHF studies contribute a lot to the development planning in Arctic territories in terms of optimization of the location of infrastructure and the sites of the mineral deposits exploration. Since the structure of the Earth's crust and upper mantle has a large impact on the formation of hydro-

carbons, GHF analysis is quite useful for identifying potential locations of hydrocarbon deposits. For example, [Khutorskoy et al. \[2013\]](#) indicate a strong relation of the thermal field and oil and gas potential in the Arctic seas. [Kharitonov \[2021\]](#) also shows existing correlation between the GHF anomalies, and specific geomorphological structures related to mantle degassing zones. The latter can be promising in search of oil and gas deposits. GHF studies are needed for adequate estimation of geothermal energy resources [[Majorowicz et al., 2009](#)], environmental risk assessments, especially in permafrost zones [e.g., [Westermann et al., 2009](#)], and for modelling of the ice sheets dynamics. GHF studies are directly related to glaciological and water resources prospecting, global ice-mass balance monitoring [[Rysgaard et al., 2018](#)] and evaluation of the sea level changes.

*Corresponding author: r.sidorov@gcras.ru

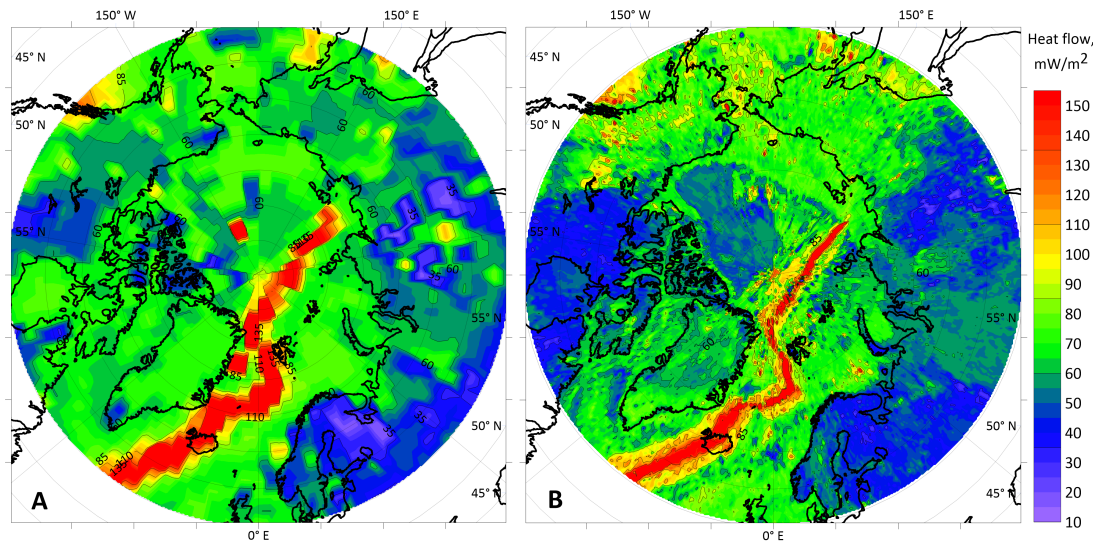


Figure 1: Arctic GHF map from the most recent global models of A: [Davies \[2013\]](#), B: [Lucaleau \[2019\]](#).

However, as it follows from the latest version of the Global Heat Flow Database maintained by the International Heat Flow Commission (IHFC), the direct measurement data on both continents and oceans have very heterogeneous coverage [[Fuchs et al., 2021](#)]. The territory of the most of the United States and Western Europe is characterized by relatively good coverage by the observational network and sufficiently high data quality. This is explained by easy accessibility of the territories. On the contrary, in the hard-to-reach regions, such as, for example, Eastern parts of Northern Eurasia, the heat flow determinations are random. The same is true for the oceans and ice-covered areas.

Reliability of the direct heat flux measurements is another important aspect of the studies. The reliability usually depends on the measurement technique and influence of external factors, such as the presence of hydrothermal circulation, permafrost, and dynamics of ice cover. For example, it was shown earlier for Greenland that climate change and, therefore, changes in ice forcing conditions, can significantly change the values of the crustal temperature gradient [[Petrunkin et al., 2013](#)]. In this case, the measured heat flow values do not reflect reliably the lithosphere thermal structure.

Since the coverage of the direct heat flow measurements is quite heterogeneous and almost absent in some areas, several methods for extrapolating GHF data are developed. The most used approach assumes that the heat flow is related to the age and structure of the lithosphere, as well as to the tectonic environment [Figure 1a](#) [e.g., [Chapman and Pollack, 1977](#); [Pollack et al., 1993](#); [Artemieva, 2006](#); [Davies and Davies, 2010](#); [Davies, 2013](#)]. Another approach is based on the global seismic model of the crust and the lithosphere for extrapolating the existing GHF data. Such approach was

proposed by [Shapiro and Ritzwoller \[2004\]](#). In recent decades, a method based on the inversion of magnetic field data for the depth to Curie point has been developed [e.g., [Maule et al., 2005](#); [Martos et al., 2017](#); [Njeudjang et al., 2020](#)]. The method allows to convert magnetic field data into a GHF map. Using the latter method, both global [[Li et al., 2017](#)] and regional GHF maps have been produced. The similarity method was adopted by applying a multiparameter approach for a large number of geophysical data by [Goutorbe et al. \[2011\]](#). They analyzed the effect of various parameters and their combination as the best proxy for use in the similarity extrapolation. Later, the method was extended for calculation of the global GHF map with the use of up to 50 parameters [Figure 1b](#) [[Lucaleau, 2019](#)].

All mentioned above methods require parameters that are often heterogeneously distributed and remain uncertain. An example of the latter is the thermal conductivity at the locations where direct heat flow measurements are present that can only be carried out near the surface. Another example is the radiogenic heat production, which is also estimated from surface measurements. The methods that use inversion of the magnetic and seismic data require many parameters, such as the distribution of magnetic properties, or velocity-to-temperature conversion factors, which are also poorly defined and depend themselves on many uncertain factors. In result, the constructed maps agree only in large scale features but differ significantly in regional and local details [Figure 1](#) [e.g., [Davies, 2013](#); [Lucaleau, 2019](#)].

In this study, we present a new approach for extrapolating the observed heat flow data based on inversion of a set of independent geophysical data. The main idea of the method is the solution of

an optimization problem by minimizing the difference between the result of solving the heat flow and the thermal equation and the observed GHF values. Furthermore, we apply this method to the Arctic zone.

2 STUDY AREA

The study area, represented by the Circumpolar zone and bounded by 55°N, includes the Arctic and the adjacent high-latitude segment (North Eurasia, North America, Greenland and Iceland territories, and the Arctic Ocean area). The Arctic Ocean area includes two major basins: the Eurasian Basin and the Amerasian Basin, divided by the Gakkel Ridge, a continuation of the Mid-Atlantic Ridge into the Arctic Ocean. To date, there are several ideas about the tectonic evolution of the Arctic region, as, despite various studies, some details of its origin remain poorly studied *Petrov et al.* [2016]. The Arctic has formed due to northward drift of the continents, which resulted in creation of the Pangea supercontinent in Late Paleozoic (Permian). Further destruction of Pangea took place in several stages during the Mesozoic (the opening of the Amerasian Basin) and Cenozoic (the opening of the Eurasian Basin). Tectonically, the Gakkel Ridge and its continuation at the Eurasian continent form a margin between the North American and Eurasian plates. This margin is characterized by relatively intense seismicity as a result of convergence tectonics between the plates [*Kanao et al.*, 2015]. Due to complicated geological history, the Arctic consists of various structures and blocks of different age from the Pre-Cambrian [*Drachev*, 2016]. According to the map of *Kashubin et al.* [2013], the overall diversity of crustal types in the Arctic includes 2 types of the oceanic crust, 5 types of the continental crust, and the crust of a transition type, represented by a local segment within the Amerasian basin. [*Kaban et al.*, 2002] distinguish a separate type for the crust segment related to Iceland, defining it as a thickened oceanic crust typical for “hot spot” segments or volcanic plateaus.

The main reference sites of the study area are, first of all, the ones in which the GHF produces local maxima or minima. Such sites are, for instance, the Iceland hot spot (local maximum), and the Anabar plateau (GHF minimum).

3 METHOD AND DATA

The expressions for the heat flow and the steady-state thermal equation in the one-dimensional case are:

$$Q = -\lambda \frac{\partial T}{\partial z}; \quad \lambda \frac{\partial T^2}{\partial z^2} = A, \quad (1)$$

where T and z are the temperature and depth, Q and λ are the heat flow and thermal conductivity, and A is the radiogenic heat production. All the parameters depend on depth. In turn, the distribution of these parameters with depth depends on the lithosphere structure and composition.

The greatest effect on the surface heat flow is produced by the thermal generation of radiogenic elements in the upper crust (A). There are two most used empirical expressions for the distribution of the parameter A with depth – constant and exponential: $A = A_0 \cdot \exp(-z/h)$, where A_0 is the radiogenic heat production at the surface and h is the reference depth of usually ±10 km [e.g., *Turcotte and Schubert*, 2003]. Such uncertainty, both in the thermal properties and vertical structure does not allow to build a robust thermal model of the crust and upper mantle.

Since the thermal equation (1) is linear, we can say that the change in the temperature gradient with depth will be equal to A/λ and the temperature gradient value near the surface can be represented by the sum of contributions of the thermal equation solutions for each depth. To compensate the data uncertainty, we introduce an additional term (R) to the right-hand side of (1):

$$\lambda \frac{\partial T^2}{\partial z^2} = A + R, \quad (2)$$

where $R(z)$ is the error-compensating empirical function.

The idea of the method is to find the parameters of this empirical correction function $R(z)$ so that the resulting solution of the thermal equation (2) has a minimum quadratic deviation from the values known from the observed data. Thus, we solve the inverse problem by minimizing the expression (3):

$$\begin{aligned} Res = & \left(\frac{w_1 \cdot (H_{100} - H_{100}^*)^2}{w_1 + w_2 + w_3 + w_4} \right. \\ & + \frac{w_2 \cdot (H_{550} - H_{550}^*)^2}{w_1 + w_2 + w_3 + w_4} \\ & + \frac{w_3 \cdot (H_{580} - H_{580}^*)^2}{w_1 + w_2 + w_3 + w_4} \\ & \left. + \frac{w_4 \cdot (H_{1175} - H_{1175}^*)^2}{w_1 + w_2 + w_3 + w_4} \right)^{1/2}. \end{aligned} \quad (3)$$

Iterating for Ax in the residual function

$$R(z) = Ax \cdot e^{-z/Hl}, \quad (4)$$

where Hl is the local lithospheric thickness.

In the (3) w_1-w_4 are weights, which in the particular case of current problem are equal to one. H_{100} , H_{550} , H_{580} , and H_{1175} are the depths of the

Table 1 : List of observables and corresponding indexes used in the (3)

Observable	Source	Index
Depth of isotherm T=100 °C from direct measurements data (where available)	IHFC Global Heat Flow Database [Fuchs et al., 2021]	H_{100}
Global Curie depth (T=550 °C)	ESM_025 model [Li et al., 2017]	H_{550}
Global continental Curie depth (T=580 °C)	[Gard and Hasterok, 2021]	H_{580}
Depth of isotherm T=1175 °C	derived from the tomography model SL2013sv [Schaeffer and Lebedev, 2013; Hoggard et al., 2020]	H_{1175}

isotherms 100 °C, 550 °C, 580 °C, and 1175 °C, derived from independent data (Table 1) which include two Curie point depth models from inversion of magnetic field data [Li et al., 2017; Gard and Hasterok, 2021], an estimate of the 1175 °C isotherm depth from seismic data [Hoggard et al., 2020], and direct heat flux measurements from the IHFC global heat flow database [Fuchs et al., 2021]. In the latter case, the 100 °C isotherm depth was calculated based on the measured GHF and thermal properties from the reference model at each point of the calculation grid. The direct measurement values presented in the Global heat flow database have a wide variation and may include negative values that are not directly related to the GHF. Such values often correspond to bottom measurements and may be related to some factors of the marine GHF measurements, for example to the hydrothermal activity in the sub-bottom layers. For this reason, for our model we use only the GHF values within the range 10–500 W/mK, averaged over areas of 50 km in diameter.

As the initial solution for the iterative inversion procedure, we use the direct heat transfer problem solution for the lithosphere according to the lithosphere model. In this model, the lithosphere structure is taken from the LITHO1.0 Figure 2 [Pasyanos et al., 2014] model, while the thermal properties of each lithospheric layer are presented by the averaged parameters Table 2. For every surface grid point we solve the thermal equation (1) by a finite difference method. As the boundary conditions, we assume a temperature of 0 °C at the surface and 1300 °C at the lithosphere-asthenosphere boundary (LAB), which depth is determined by the litho-

sphere thickness (Figure 2d). Strictly speaking, the LAB which is defined by seismic methods, should not necessarily coincide with the boundary of the thermal lithosphere [e.g., Artemieva, 2009], but we use it because neither the LAB depth nor the temperature at this boundary are reliably defined by geophysical data.

The calculations were performed on a grid with a step of approximately 100 km. As can be seen from Figure 3, the initial GHF model shows a good agreement with the observed data (dots in Figure 3) in many areas, although only averaged parameters of thermal properties of the lithosphere were employed. However, significant deviations of the model from the observations are also visible, for example, in the North Atlantic, Greenland, in some parts of North America, and in the Kara and White seas. The significant deviation of the anomalous zone of increased heat flux from the rift axis in the North Atlantic, where it is assumed, can be related to the LAB map that was used in the model (Figure 2d). In the further steps, the initial model is improved by solving the optimization problem described above.

4 RESULTS

The map of the calculated pre-exponential term Ax for the error-compensating empirical function (4) shows the areas where the reference model correction is necessary (Figure 4a). This correction is relatively small in the continental regions, except for Eastern Siberia and Alaska. In general, the resulting GHF distribution corresponds to the typical values for different lithosphere types.

Table 2 : Thermal properties used for the reference model

Parameter	Sediments	Upper crust	Lower crust	Lith. mantle
Thermal conductivity λ , W/mK	2.2	Depends on temperature and pressure [Förster et al., 2010]		
Radiogenic heat production A, $\mu\text{W}/\text{m}^3$	1	$2.5 \cdot \exp\left(-\frac{z}{10^3}\right)$	0.1	4E-3

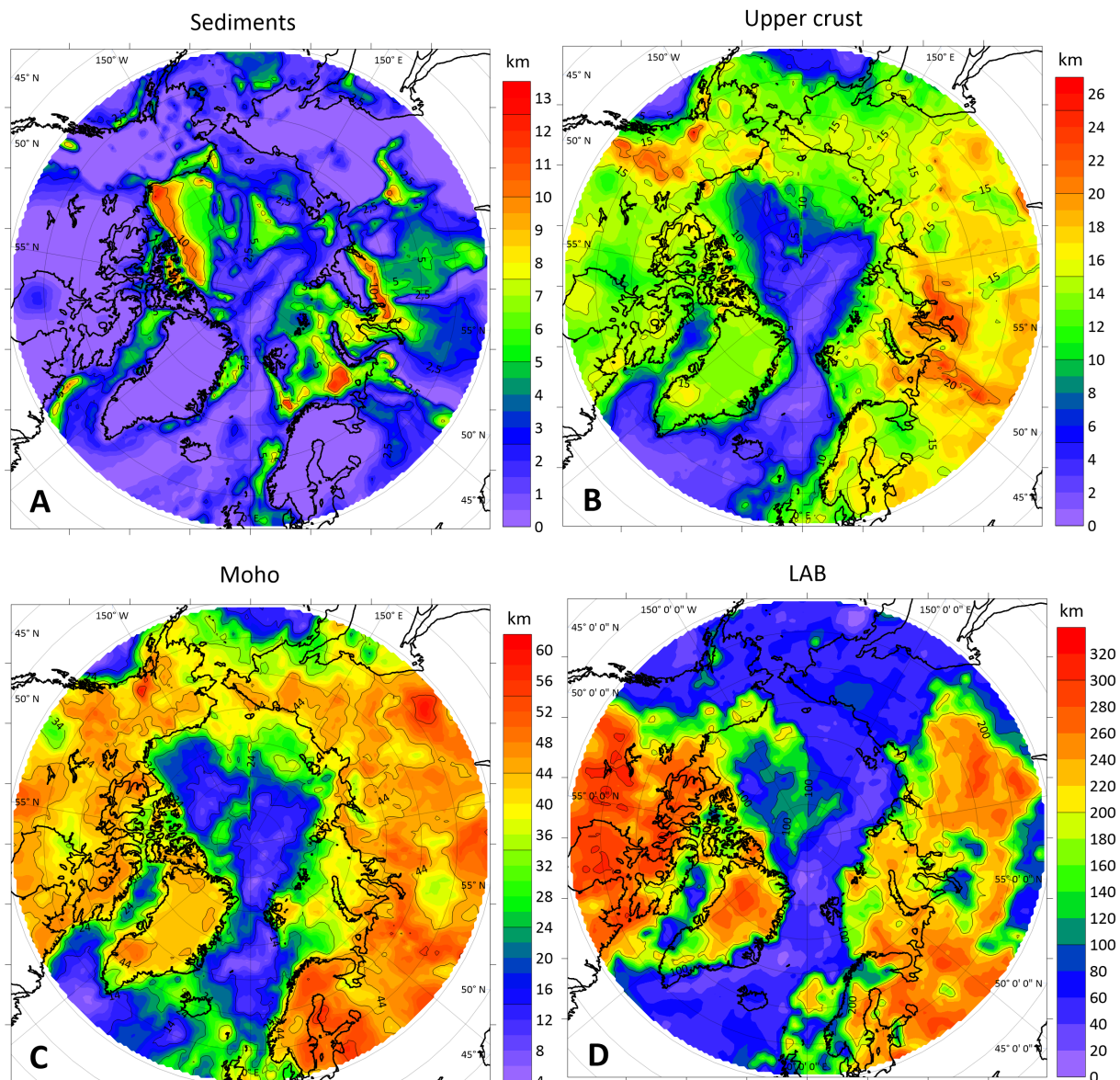


Figure 2: The data set used to calculate the reference model LITHO1.0 [Pasyanos et al., 2014]: sedimentary thickness (a), upper crust (b), the Moho depth (c), and depth of the lithosphere-asthenosphere boundary (d). All data is corrected for topography and presented in Arctic-stereographic projection.

The areas of the ancient East European, Siberian, North American cratons generally correspond to large zones of relatively low ($30\text{--}50\text{ mW/m}^2$) heat flux values. The old folded belts, such as the Scandinavian-Caledonian Orogen at the north-western part of the Scandinavian Peninsula and the easternmost part of Greenland (formed during Silurian to Devonian time) or the Ural mountain belt (formed in the Late Carboniferous and Permian), are characterized by GHF values of about $50\text{--}60\text{ mW/m}^2$. The Mesozoic and Cenozoic orogeny have the GHF values more than $60\text{--}65\text{ mW/m}^2$. For the oceans, especially on the mid-ocean ridges (MORs), subduction zones, the correction for the initial model is significant. Also, significant corrections are found for the Bering Sea

in the Bering Strait area, the Komandorski basin and the westernmost part of the Aleutian basin (adjacent to the former accretionary prism of the Anadyr-Koryak folded system). The zone of positive correction in the Bering Sea partially matches the Aleutian basin. However, the GHF maximum is closer to the continental parts of Chukotka and Alaska where the heat flow reaches 110 mW/m^2 . The results of previous studies show no local maximum, except of [Langseth et al., 1980] reporting a slight uprising trend towards the Bering Sea shelf.

Significant variations in the MOR areas could be due to a combination of several factors, such as the difference in methods and the heterogeneity of the data used. These data have different resolutions, whereas in the reference model based

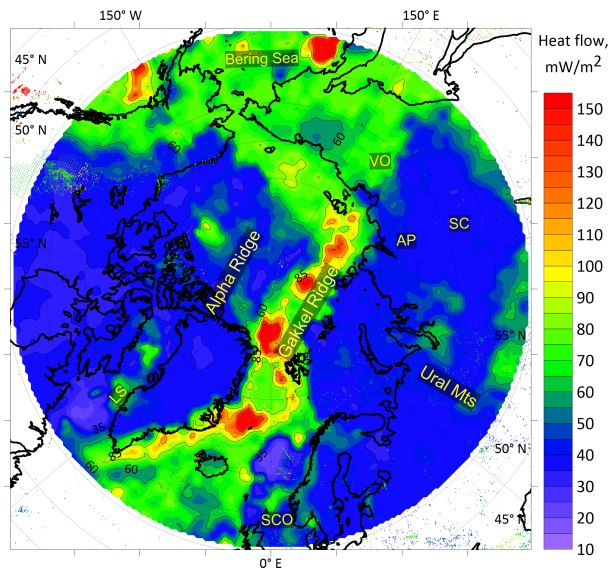


Figure 3: The initial GHF map based on the initial model of the lithosphere. The dots show the location and value of the direct heat flow measurements (IHFC 2021 database [Fuchs et al., 2021]). Here and in subsequent figures the following abbreviations are used to denote the following geographical objects and geological structures: SC – Siberian Craton; AP – Anabar Plateau; VO – Verkhoyansk Orogen; SCO – Scandinavian Caledonian Orogen; LS – Labrador Sea.

on LITHO1.0 (Figure 2 [Pasyanos et al., 2014]), the resolution is the same for all components. Because the lithospheric thickness has a large gradient across the axial zones of MORs, the value of the pre-exponential coefficient can change sign even over a short distance to compensate for the resolution mismatch in the data used for the inversion. The amplitude of the term is also most significant for this area. However, the resulting values for MOR demonstrate a good correlation both with the values of the direct GHF measurements (colored dots in Figure 4b), and with the location of active hydrothermal vents (blue stars in Figure 4b). It is noteworthy that the reference model was also adjusted for the North Atlantic south of Iceland. The continental rift separating the Verkhoyansk-Kolyma Plate and the Siberian Craton becomes more prominent as the zone with the increased up to 70–90 mW/m² heat flow. This feature is either absent (Figure 1b) or weakly expressed (Figure 1a) in the previous models of the global GHF. Within the Verkhoyansk orogeny area in its Arctic part the GHF values correlate with the Moho depth variations. The local minimum of 60 mW/m² corresponds to the Moho depths 28–30 km, according to the Moho map by [Kaban et al., 2022], and the local maximum about 90 mW/m² is associated with the Moho depths 40–45 km. The latter can be ex-

plained by a thicker upper crust enriched in radiogenic elements that make a significant contribution to the surface heat flow.

The shape of the heat flow anomalies in Greenland generally resembles the results obtained earlier by a joint modeling of the glacier dynamics, basal melting and the lithosphere thermo-mechanical model [Rogozhina et al., 2016] and the thermal isostasy method [Artemieva, 2019], although slightly lower in amplitude. Next, the lower heat flow (60 mW/m² maximum comparing to 80–90 mW/m² in the initial map) is identified in the new map for two spots related to the Labrador Sea (separating the Greenland plate and the North American plate). Moreover, the mentioned GHF anomalies have changed their shape: in the new map they represent an elongated 50–60 mW/m² zone bounding the western Greenland coast in the Labrador Sea. The GHF anomalies in the new map better match the detailed crustal thickness and LAB depth maps for the Labrador Sea region provided by [Peace et al., 2017] than the ones on the initial map. However, the new GHF map does not reflect the details of the mentioned maps south of Greenland. A zone within the Greenland Caledonian orogeny, closest to the MOR, displays the values 65–100 mW/m², which can be explained by the Iceland plume impact.

The large zone of heat flow values 70–80 mW/m² is associated with several crustal types. In the vicinity of MOR, this zone is related to the normal oceanic crust typical for spreading conditions. However, in the Eastern Asia Arctic these values correspond to the thinned continental crust [Kashubin et al., 2013], typical for the Arctic shelf seas (Laptev Sea, East Siberian Sea and Chukchi sea). Note that for the crust of the same type underlying the Arctic seas west of the Gakkel Ridge (e.g., Kara and Barents Seas) the GHF values are much lower due to the older lithosphere, significant thickness of sediments, and difference in the upper crustal layer thickness. The cratons and old fold belts are characterized by low GHF values. The new GHF map also displays about 10 mW/m² higher GHF magnitudes for the northern part of the Amerasian basin, indicating the Alpha Ridge, a part of the Alpha-Mendeleev large igneous province [Drachev, 2016]. Therefore, the map correlates both with the lithosphere age and structure in a combined way.

The map also matches the instrumental heat flow measurements in some locations in the continental Arctic. For example, it agrees with most of the borehole heat flow measurements in the Yamal Peninsula [Isaev et al., 2019], which are about 47 to 62 mW/m². The local GHF minimum in the northern part of the Siberian craton shows the position of another reference site – the Anabar shield,

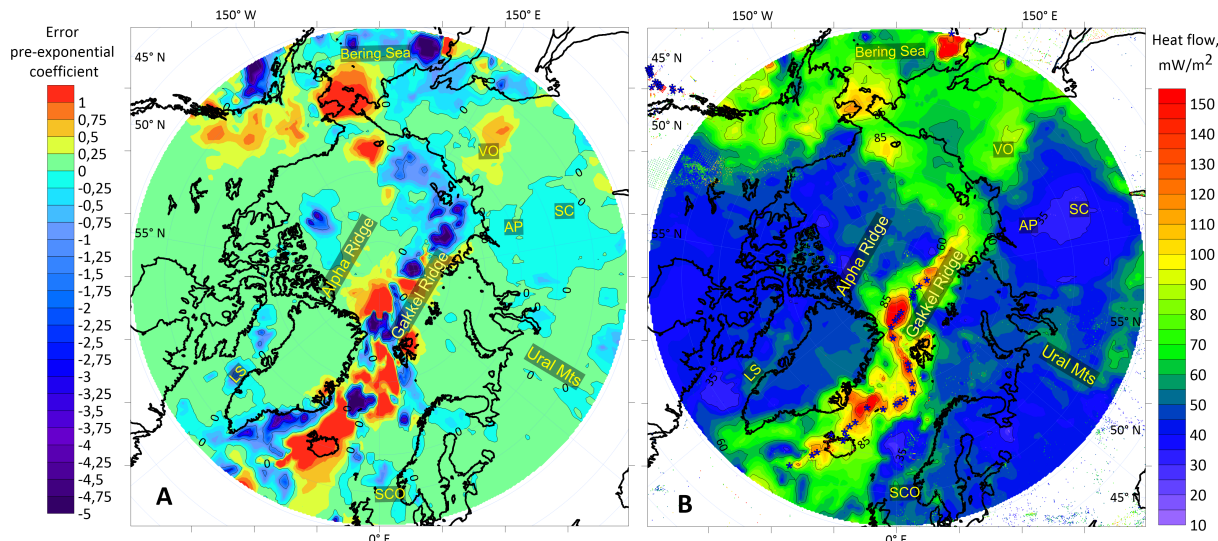


Figure 4: Map of the pre-exponential term Ax in (4) (a) and the resulting GHF map for the Arctic region (b). The dots show the location and value of the direct heat flow measurements (IHFC 2021 database [Fuchs et al., 2021]). Blue stars indicate locations of submarine active vent fields (InterRidge global database v. 3.2 [Beaulieu et al., 2013]).

characterized by extremely low heat flow values of about 20 mW/m^2 in its central part to 35 mW/m^2 in the folded rocks at its edges [Milanovskiy et al., 2017].

5 DISCUSSION

In a recent study, [Lucazeau, 2019] discussed in details the factors that affect the accuracy of the similarity-based methods. This study demonstrates that the sedimentation processes, heterogeneous distribution of radiogenic elements in the crust, different conditions at divergent boundaries, etc. can affect the surface heat flow more strongly than the lithosphere age, even considering the statistical deviations accepted within the similarity method. The studies of Goutorbe et al. [2011] and Lucazeau [2019] concluded that various independent data should be considered for a more reliable GHF extrapolation. They also pointed that all similarity methods, as well as the heat flux estimates for the ocean floor based on the oceanic plate thermal models cannot provide sufficiently reliable results. The method proposed in this paper allows to find a solution that satisfies any available data set without using critical, but often unreliable parameters, such as, for example, the distribution of the radiogenic elements in the crust. In further development, the reference model can be built considering a more accurate distribution of the thermal properties of the crust and lithosphere, and the target function can be augmented with heterogeneously distributed data, such as the temperature estimates from thermobarometric analysis of xenoliths.

The suggested method is simple and flexible, but also has several limitations. In particular, the error-compensating function $R(z)$ (2) is rather empirical and requires further development, and the choice of this function can significantly affect the result. In our case, this function operates with one variable, which limits its application since the curvature of the function remains constant. It is more reasonable to use the optimization method with two or more variables. This would allow to satisfy the data in the target function (3) more accurately. The selection of the weight parameters in the target function is also empirical. It depends on the assessment of the data quality used in the model, which is not always possible to determine reliably. It should also be taken into account that when using several databases obtained by similar methods (e.g., determining the Curie point from inversion of magnetic field data), these data will have a greater contribution to the final solution. This should be considered when estimating weights parameters.

6 CONCLUSIONS

This study presents a new method for inverting geophysical data based on the solution of an optimization problem. Although we employ a simplified version of the method, it has been demonstrated that it has good potential for further development. The advantage of the method is relative ease of its implementation and the possibility of adjusting the data, the reliability of which is hard to assess. As the result of the first application, we obtained the GHF map for the Arctic region, which correlates well with the direct heat flux measure-

ments and the structure, tectonic type and age of the lithosphere. This method allows direct estimation of the GHF on the mid-ocean ridges, whereas most studies are based on the models of thermal evolution depending on the age of the lithosphere. The resulting heat flow map along the mid-ocean ridge coincides well with the location of active hydrothermal vents, which confirms reliability of the new model for this area. We consider this study as a basis for further development of the method that allows not only to estimate the surface GHF, but also to calculate the entire geotherm for the lithosphere.

7 DATA AVAILABILITY

All the datasets presented here are based on the initial data from public domain resources. The obtained results, including the new GHF model and the pre-exponential term data, will soon be available at the World Data Center for Solid Earth Physics Physics website http://www.wdcb.ru/arctic_antarctic/arctic_hf_1.html.

Acknowledgements. The authors are grateful to Dr. M. K. Kaban for his valuable contributions at all stages of this research. Also the authors would like to thank two anonymous reviewers for taking time and effort to review our manuscript and make valuable remarks and comments that helped us to improve the manuscript. This research was funded by the Russian Science Foundation (project No. 21-77-30010).

REFERENCES

- Artemieva, I. M., Global $1^\circ \times 1^\circ$ thermal model tc1 for the continental lithosphere: Implications for lithosphere secular evolution, *Tectonophysics*, 416(1), 245–277, doi:<https://doi.org/10.1016/j.tecto.2005.11.022>, the Heterogeneous Mantle, 2006.
- Artemieva, I. M., The continental lithosphere: Reconciling thermal, seismic, and petrologic data, *Lithos*, 109(1-2), 23–46, doi:[10.1016/j.lithos.2008.09.015](https://doi.org/10.1016/j.lithos.2008.09.015), 2009.
- Artemieva, I. M., Lithosphere thermal thickness and geothermal heat flux in Greenland from a new thermal isostasy method, *Earth-Science Reviews*, 188, 469–481, doi:[10.1016/j.earscirev.2018.10.015](https://doi.org/10.1016/j.earscirev.2018.10.015), 2019.
- Beaulieu, S. E., E. T. Baker, C. R. German, and A. Maffei, An authoritative global database for active submarine hydrothermal vent fields, *Geochemistry, Geophysics, Geosystems*, 14(11), 4892–4905, doi:[10.1002/2013gc004998](https://doi.org/10.1002/2013gc004998), 2013.
- Chapman, D. S., and H. N. Pollack, Regional geotherms and lithospheric thickness, *Geology*, 5(5), 265–268, doi:[10.1130/0091-7613\(1977\)5<265:RGALT>2.0.CO;2](https://doi.org/10.1130/0091-7613(1977)5<265:RGALT>2.0.CO;2), 1977.
- Davies, J. H., Global map of solid Earth surface heat flow, *Geochemistry, Geophysics, Geosystems*, 14(10), 4608–4622, doi:<https://doi.org/10.1002/ggge.20271>, 2013.
- Davies, J. H., and D. R. Davies, Earth's surface heat flux, *Solid Earth*, 1(1), 5–24, doi:[10.5194/se-1-5-2010](https://doi.org/10.5194/se-1-5-2010), 2010.
- Drachev, S. S., Fold belts and sedimentary basins of the Eurasian Arctic, *arktos*, 2(1), doi:[10.1007/s41063-015-0014-8](https://doi.org/10.1007/s41063-015-0014-8), 2016.
- Fuchs, S., B. Norden, and International Heat Flow Commission, The global heat flow database: Release 2021, *GFZ Data Services*, doi:[10.5880/FIDGEO.2021.014](https://doi.org/10.5880/FIDGEO.2021.014), 2021.
- Förster, H.-J., A. Förster, R. Oberhänsli, and D. Stromeyer, Lithospheric composition and thermal structure of the Arabian Shield in Jordan, *Tectonophysics*, 481(1-4), 29–37, doi:[10.1016/j.tecto.2008.11.014](https://doi.org/10.1016/j.tecto.2008.11.014), 2010.
- Gard, M., and D. Hasterok, A global Curie depth model utilising the equivalent source magnetic dipole method, *Physics of the Earth and Planetary Interiors*, 313, 106672, doi:[10.1016/j.pepi.2021.106672](https://doi.org/10.1016/j.pepi.2021.106672), 2021.
- Goutorbe, B., J. Poort, F. Lucaleau, and S. Raillard, Global heat flow trends resolved from multiple geological and geophysical proxies, *Geophysical Journal International*, 187(3), 1405–1419, doi:[10.1111/j.1365-246x.2011.05228.x](https://doi.org/10.1111/j.1365-246x.2011.05228.x), 2011.
- Hoggard, M. J., K. Czarnota, F. D. Richards, D. L. Huston, A. L. Jaques, and S. Ghelichkhan, Global distribution of sediment-hosted metals controlled by craton edge stability, *Nature Geoscience*, 13(7), 504–510, doi:[10.1038/s41561-020-0593-2](https://doi.org/10.1038/s41561-020-0593-2), 2020.
- Isaev, V. I., G. A. Lobova, A. N. Fomin, V. I. Bulatov, S. G. Kuzmenkov, M. F. Galieva, and D. S. Krutenko, Heat flow and presence of oil and gas (the Yamal peninsula, Tomsk region), *Georesursy*, 21(3), 125–135, doi:[10.18599/grs.2019.3.125-135](https://doi.org/10.18599/grs.2019.3.125-135), 2019.
- Kaban, M. K., Ó. G. Flóvenz, and G. Pálmasón, Nature of the crust-mantle transition zone and the thermal state of the upper mantle beneath Iceland from gravity modelling, *Geophysical Journal International*, 149(2), 281–299, doi:[10.1046/j.1365-246x.2002.01622.x](https://doi.org/10.1046/j.1365-246x.2002.01622.x), 2002.
- Kaban, M. K., P. Schwintzer, I. M. Artemieva, and W. D. Mooney, Density of the continental roots: compositional and thermal contributions, *Earth and Planetary Science Letters*, 209(1-2), 53–69, doi:[10.1016/s0012-821x\(03\)00072-4](https://doi.org/10.1016/s0012-821x(03)00072-4), 2003.
- Kaban, M. K., R. V. Sidorov, A. A. Soloviev, A. D. Gvishiani, A. G. Petrunin, O. V. Petrov, S. N. Kashubin, E. A. Androsov, and E. D. Milshtein, A New Moho Map for North-Eastern Eurasia Based on the Analysis of Various Geophysical Data, *Pure and Applied Geophysics*, doi:[10.1007/s00024-021-02925-6](https://doi.org/10.1007/s00024-021-02925-6), 2022.

- Kanao, M., V. D. Suvorov, S. Toda, and S. Tsuboi, Seismicity, structure and tectonics in the Arctic region, *Geoscience Frontiers*, 6(5), 665–677, doi:[10.1016/j.gsf.2014.11.002](https://doi.org/10.1016/j.gsf.2014.11.002), 2015.
- Kashubin, S., N. Pavlenkova, O. Petrov, E. Milshtein, S. Shokalsky, and Y. Erinchev, Crustal types in the Circumpolar Arctic, *Regional Geology and Metallogeny*, 55, 5–20, 2013.
- Kharitonov, A. L., Geophysical studies of ring structures for the search for oil and gas deposits, *Bulletin of Udmurt University. Series Biology. Earth Sciences*, 31(3), 319–328, doi:[10.35634/2412-9518-2021-31-3-319-328](https://doi.org/10.35634/2412-9518-2021-31-3-319-328), 2021.
- Khutorskoy, M. D., V. R. Akhmedzyanov, A. V. Ermakov, Y. G. Leonov, L. V. Podgornykh, B. G. Polyak, E. A. Sukhikh, and L. A. Tsibulya, *Geothermics of the Arctic seas*, 230 pp., GEOS, Moscow, (In Russian), 2013.
- Langseth, M. G., M. A. Hobart, and K. iti Horai, Heat flow in the Bering Sea, *Journal of Geophysical Research: Solid Earth*, 85(B7), 3740–3750, doi:[10.1029/jb085ib07p03740](https://doi.org/10.1029/jb085ib07p03740), 1980.
- Li, C.-F., Y. Lu, and J. Wang, A global reference model of Curie-point depths based on EMAG2, *Scientific Reports*, 7(1), 45129, doi:[10.1038/srep45129](https://doi.org/10.1038/srep45129), 2017.
- Lucazeau, F., Analysis and Mapping of an Updated Terrestrial Heat Flow Data Set, *Geochemistry, Geophysics, Geosystems*, 20(8), 4001–4024, doi:[10.1029/2019gc008389](https://doi.org/10.1029/2019gc008389), 2019.
- Majorowicz, J., S. E. Grasby, and W. R. Skinner, Estimation of Shallow Geothermal Energy Resource in Canada: Heat Gain and Heat Sink, *Natural Resources Research*, 18(2), 95–108, doi:[10.1007/s11053-009-9090-4](https://doi.org/10.1007/s11053-009-9090-4), 2009.
- Martos, Y. M., M. Catalán, T. A. Jordan, A. Golynsky, D. Golynsky, G. Eagles, and D. G. Vaughan, Heat flux distribution of antarctica unveiled, *Geophysical Research Letters*, 44(22), 11,417–11,426, doi:<https://doi.org/10.1002/2017GL075609>, 2017.
- Maule, C. F., M. E. Purucker, N. Olsen, and K. Mosegaard, Heat Flux Anomalies in Antarctica Revealed by Satellite Magnetic Data, *Science*, 309(5733), 464–467, doi:[10.1126/science.1106888](https://doi.org/10.1126/science.1106888), 2005.
- Milanovskiy, S. Y., M. K. Kaban, O. M. Rozen, and A. V. Egorkin, Gophysical features of the Anabar shield crust, *Bulletin of Kamchatka Regional Association «Educational-Scientific Center»: Earth Sciences*, 4, 56–71, (in Russian), 2017.
- Njeudjang, K., J. D. Kana, A. Tom, J. M. A. Essi, N. Djongyang, and R. Tchinda, Curie point depth and heat flow deduced from spectral analysis of magnetic data over Adamawa volcanic region (Northern Cameroon): geothermal implications, *SN Applied Sciences*, 2(8), doi:[10.1007/s42452-020-3099-z](https://doi.org/10.1007/s42452-020-3099-z), 2020.
- Pasyanos, M. E., T. G. Masters, G. Laske, and Z. Ma, LITHO1.0: An updated crust and lithospheric model of the Earth, *Journal of Geophysical Research: Solid Earth*, 119(3), 2153–2173, doi:[10.1002/2013jb010626](https://doi.org/10.1002/2013jb010626), 2014.
- Peace, A. L., G. R. Foulger, C. Schiffer, and K. J. McCaffrey, Evolution of labrador sea–baffin bay: Plate or plume processes?, *Geoscience Canada*, 44(3), 91–102, doi:[10.12789/geocanj.2017.44.120](https://doi.org/10.12789/geocanj.2017.44.120), 2017.
- Petrov, O., A. Morozov, S. Shokalsky, S. Kashubin, I. M. Artemieva, N. Sobolev, E. Petrov, R. E. Ernst, S. Sergeev, and M. Smelror, Crustal structure and tectonic model of the Arctic region, *Earth-Science Reviews*, 154, 29–71, doi:<https://doi.org/10.1016/j.earscirev.2015.11.013>, 2016.
- Petrunin, A. G., I. Rogozhina, A. P. M. Vaughan, I. T. Kukkonen, M. K. Kaban, I. Koulakov, and M. Thomas, Heat flux variations beneath central greenland's ice due to anomalously thin lithosphere, *Nature Geoscience*, 6(9), 746–750, doi:[10.1038/ngeo1898](https://doi.org/10.1038/ngeo1898), 2013.
- Pollack, H. N., S. J. Hurter, and J. R. Johnson, Heat flow from the Earth's interior: Analysis of the global data set, *Reviews of Geophysics*, 31(3), 267–280, doi:[10.1029/93RG01249](https://doi.org/10.1029/93RG01249), 1993.
- Rogozhina, I., A. G. Petrunkin, A. P. M. Vaughan, B. Steinberger, J. V. Johnson, M. K. Kaban, R. Calov, F. Rickers, M. Thomas, and I. Koulakov, Melting at the base of the greenland ice sheet explained by iceland hotspot history, *Nature Geoscience*, 9(5), 366–369, doi:[10.1038/ngeo2689](https://doi.org/10.1038/ngeo2689), 2016.
- Rysgaard, S., J. Bendtsen, J. Mortensen, and M. K. Sejr, High geothermal heat flux in close proximity to the Northeast Greenland Ice Stream, *Scientific Reports*, 8(1), doi:[10.1038/s41598-018-19244-x](https://doi.org/10.1038/s41598-018-19244-x), 2018.
- Schaeffer, A. J., and S. Lebedev, Global shear speed structure of the upper mantle and transition zone, *Geophysical Journal International*, 194(1), 417–449, doi:[10.1093/gji/ggt095](https://doi.org/10.1093/gji/ggt095), 2013.
- Shapiro, N. M., and M. H. Ritzwoller, Inferring surface heat flux distributions guided by a global seismic model: particular application to Antarctica, *Earth and Planetary Science Letters*, 223(1), 213–224, doi:<https://doi.org/10.1016/j.epsl.2004.04.011>, 2004.
- Turcotte, D. L., and G. Schubert, Geodynamics, *Journal of Fluid Mechanics*, 477, 410–411, doi:[10.1017/S0022112002223708](https://doi.org/10.1017/S0022112002223708), 2003.
- Westermann, S., J. Lüers, M. Langer, K. Piel, and J. Boike, The annual surface energy budget of a high-arctic permafrost site on Svalbard, Norway, *The Cryosphere*, 3(2), 245–263, doi:[10.5194/tc-3-245-2009](https://doi.org/10.5194/tc-3-245-2009), 2009.